Author(s): Tossavainen, Helena; Aitio, Olli; Hellman, Maarit; Saksela, Kalle; Permi, Perttu

Title: Structural Basis of the High Affinity Interaction between the Alphavirus Nonstructural Protein-3 (nsP3) and the SH3 Domain of Amphiphysin-2

Year: 2016

Version:

Please cite the original version:

Tossavainen, H., Aitio, O., Hellman, M., Saksela, K., & Permi, P. (2016). Structural Basis of the High Affinity Interaction between the Alphavirus Nonstructural Protein-3 (nsP3) and the SH3 Domain of Amphiphysin-2. Journal of Biological Chemistry, 291(31), 16307-16317. https://doi.org/10.1074/jbc.M116.732412

THE JOURNAL OF BIOLOGICAL CHEMISTRY VOL. 291, NO. 31, pp. 16307–16317, July 29, 2016

Structural Basis of the High Affinity Interaction between the *Alphavirus* Nonstructural Protein-3 (nsP3) and the SH3 Domain of Amphiphysin-2*[S]

Received for publication, April 13, 2016, and in revised form, May 31, 2016 Published, JBC Papers in Press, June 6, 2016, DOI 10.1074/jbc.M116.732412

Helena Tossavainen[‡1], **Olli Aitio**[‡1,2], **Maarit Hellman**[‡1,3], **Kalle Saksela**[§], **and Perttu Permi**[‡¶4]

From the [‡]*Program in Structural Biology and Biophysics, Institute of Biotechnology, University of Helsinki and the* [§]*Department of Virology, University of Helsinki and Helsinki University Hospital, FI-00014 Helsinki, Finland and the* [¶]*Departments of Biological and Environmental Science and Chemistry, Nanoscience Center, University of Jyvaskyla, FI-40014 Jyvaskyla, Finland*

We show that a peptide from Chikungunya virus nsP3 protein spanning residues 1728–1744 binds the amphiphysin-2 (BIN1) Src homology-3 (SH3) domain with an unusually high affinity (K_d 24 nM). Our NMR solution complex structure together with isothermal titration calorimetry data on several related viral and cellular peptide ligands reveal that this exceptional affinity originates from interactions between multiple basic residues in the target peptide and the extensive negatively charged binding surface of amphiphysin-2 SH3. Remarkably, these arginines show no fixed conformation in the complex structure, indicating that a transient or fluctuating polyelectrostatic interaction accounts for this affinity. Thus, via optimization of such dynamic electrostatic forces, viral peptides have evolved a superior binding affinity for amphiphysin-2 SH3 compared with typical cellular ligands, such as dynamin, thereby enabling hijacking of amphiphysin-2 SH3-regulated host cell processes by these viruses. Moreover, our data show that the previously described consensus sequence P*X*RP*X*R for amphiphysin SH3 ligands is inaccurate and instead define it as an extended Class II binding motif P*XX*P*X*Rp*X*R, where additional positive charges between the two constant arginine residues can give rise to extraordinary high SH3 binding affinity.

Src homology 3 (SH3)[5] domains are highly abundant, conserved, non-catalytic structural modules that are utilized as building blocks to target proline-rich sequences in various modular proteins (1). Despite their small size of ~60 residues, SH3 domains bind a myriad of small linear motifs (SLiMs) found predominantly in signaling pathways (2). SLiMs are sequences of ~3–10 amino acid residues typically located in intrinsically disordered regions of proteins, which may become structured upon binding. This entropically unfavorable disorder-to-order transition upon binding permits transient interactions of relatively low affinity but high specificity. In the context of complex signaling networks, decoupling affinity from specificity brings in functional advantages, as both rapid association and dissociation are required. Intracellular signaling is typically under tight regulation. Tightly regulated processes are frail and constantly targeted by various pathogens, which mimic the SLiMs and are able to hijack (or disconnect) part of the signaling pathway to their own needs by fine-tuning of amino acid composition of the pathogenic effector (3).

SH3 domains share a common β-barrel structure composed of five β strands connected by RT, n-Src, and distal loops and a short 3_{10} helix. A structurally conserved, hydrophobic SLiM binding site resides on the surface of the domain, to which a peptide binds commonly in a left-handed type II (PPII) polyproline helix conformation in either of two opposite orientations. Consensus sequences typically recognized by SH3 domains are $+X\phi$PXXP (Class I) and XP$X\phi$P$X+$ (Class II) where $+$, ϕ, and X signify R/K, hydrophobic, and any residue, respectively. The positively charged residue governs the orientation of the peptide in the complex. In addition to the conserved interaction, binding affinity can be modulated through concurrent interactions with divergent specificity determining regions (1).

Amphiphysin-2/BIN1 has key roles in regulation of endocytosis and membrane recycling, cytoskeleton regulation, DNA repair, cell cycle progression, and apoptosis (for a review, see Ref. 4). It is widely expressed in different tissues in >10 isoforms. All isoforms have in common an N-terminal BAR (BIN/amphiphysin/Rvs) domain capable of forming crescent-shaped dimers and sensing and inducing membrane curvature (5) and a C-terminal SH3 domain. Amphiphysin SH3 domain (referred hereafter to as amp-SH3) interacts among others with dynamin (6) and synaptojanin (7) in receptor-induced endocytosis and with c-Myc, a regulator of cell proliferation, growth, differentiation, and apoptosis (8).

Recently it was shown that amphiphysin is targeted by several alphaviruses (9), the genus containing ~30 members including Chikungunya (CHIKV), Semliki forest (SFV), and

* The authors declare that they have no conflicts of interest with the contents of this article.

[S] This article contains supplemental Figs. 1 and 2.

The atomic coordinates and structure factors (code 5I22) have been deposited in the Protein Data Bank (http://wwpdb.org/).

The atomic coordinates, structural restraints, and chemical shifts (30010) have been deposited in Biological Magnetic Resonance Data Bank.

[1] These authors contributed equally to this work.

[2] Present address: Glykos Finland Ltd., Viikinkaari 6, FI-00790 Helsinki, Finland.

[3] Present address: Dept. of Chemistry, Nanoscience Center, University of Jyvaskyla, FI-40014 Finland.

[4] To whom correspondence should be addressed: P. O. Box 35, University of Jyvaskyla, FI-40014 Finland. Tel.: 358-40-8054288; E-mail: perttu.permi@jyu.fi.

[5] The abbreviations used are: SH3, Src homology 3; SLiM, small linear motif; CHIKV, Chikungunya; nsP3, nonstructural protein-3; SFV, Semliki forest; HCV, hepatitis C virus; ITC, isothermal titration calorimetry; CSP, chemical shift perturbation; HSQC, heteronuclear single quantum correlation; r.m.s.d., root mean square deviation(s); CD2AP, CD2-associated protein; RT, room temperature.

Sindbis viruses. *Alphavirus* RNA replication takes place in small membrane invaginations, spherules, protruding initially from the surface of the plasma membrane and at a later stage of the infection from the surface of cytopathic vacuoles type I (10). The latter are modified endo- and lysosomes with the viral replication complex consisting of nonstructural proteins nsP1-nsP4 on their surface. The role of nsP3 in the replication complex remains less clear. It has three domains, the N-terminal macrodomain with phosphatase activity and nucleic acid binding ability, the *Alphavirus* unique domain, and the hypervariable C-terminal region. Mutational studies focused on the structurally conserved N-terminal macrodomain have pinpointed its role in RNA synthesis (11). Despite its poor conservation, the C-terminal tail region of nsP3 is essential for virulence of alphaviruses (12). Interestingly, nsP3 C-terminal domain harbors a conserved proline-rich motif (P(I/V)(P/A)PPR) that targets the SH3 domain of amphiphysin. This proline-rich region recruits the amp-SH3 to the site of viral replication complex, and mutation of Arg with Glu completely abolishes the interaction with amp-SH3 and drastically suppressed the virus replication *in vitro* (9).

Remarkably, a similar P(I/V)(P/A)PPR motif is found in the NS5A protein of hepatitis C virus (HCV), which also has been reported as a ligand for amp-SH3 (13). HCV belongs to flaviviruses and is thus very different from alphaviruses. However, it is also a positive-strand RNA virus adapted to replication within membranous structures appearing in infected cells (14). Interestingly, this viral amp-SH3 binding motif is markedly different from the P*X*RP*X*R consensus motif reported for cellular amp-SH3 ligands (7, 15), of which dynamin is perhaps the best characterized example (16).

In this work we have employed solution state NMR spectroscopy to solve the structure of amp-SH3 in complex with CHIKV nsP3. Further characterization using NMR, isothermal titration calorimetry (ITC), site-directed mutagenesis, and bioinformatics indicate that the SH3 binding epitope in dynamin is larger than previously described and that binding sites of the cellular ligand dynamin and viral proteins on amp-SH3 are similar. Mimicking the dynamin proline-rich motif permits alphaviruses to recruit amphiphysin to the viral replication complex. Through binding epitope fine-tuning alphaviruses obtain, however, a drastically higher affinity to amp-SH3.

Results

C-terminal Tail of Dynamin Is Disordered and Binds amp-SH3 with Relatively Low Affinity—Analysis of dynamin using bioinformatics tools reveals that its C-terminal tail, devoid of any secondary structure, is predicted to belong to the class of intrinsically disordered regions (see Fig. 2*A*). To characterize the interaction between dynamin and amp-SH3, we produced a 29-residue dynamin peptide (dynamin hereafter) from its C-terminal tail, ^{820}GASPDPFGPPPQV**PSRPNR**APPGV-PSRSG^{848}, which contains the previously defined P*X*RP*X*R epitope shown to be essential for amp-SH3 recognition (15, 16). See Fig. 1 for the sequence alignment of all peptides used and discussed. We performed a peptide binding assay in which unlabeled dynamin was titrated into ^{15}N-labeled amp-SH3, and binding-induced chemical shift perturbations (CSPs) were

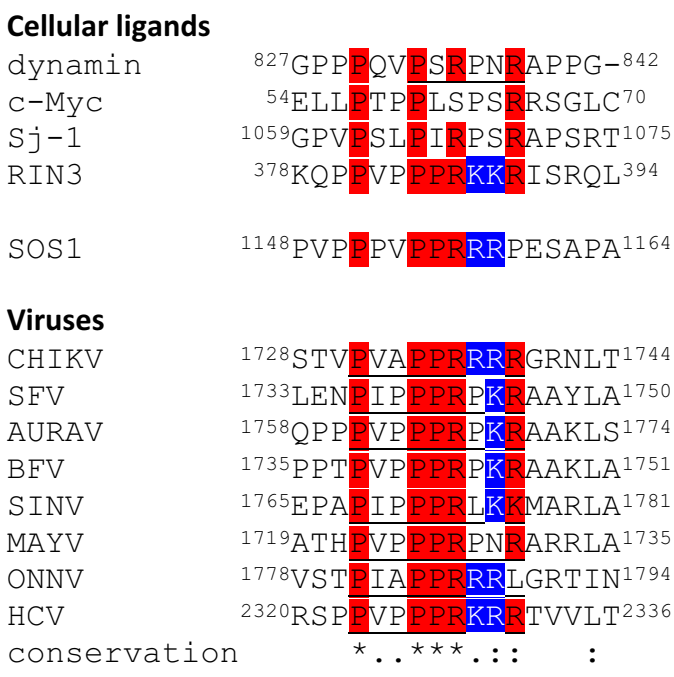

FIGURE 1. **Alignment of cellular and viral amp-SH3 ligands.** Abbreviations for cellular ligands: c-Myc, Myc proto-oncogene protein; *Sj-1*, synaptojanin 1; *RIN3*, Ras/Rab interactor. Abbreviations for viruses: *CHIKV*, Chikungunya virus; *SFV*, Semliki forest virus; *AURAV*, Aura virus; *BFV*, Barmah forest virus; *SINV*, Sindbis virus; *MAYV*, Mayaro virus; *ONNV*, O'Nyong Nyong virus (all alphaviruses); *SOS1*, Son of Sevenless 1, is a canonical Class II SH3 domain binder.

monitored using the ^{1}H,^{15}N HSQC NMR experiment. It was observed that peaks shifted linearly with the addition of peptide, indicating a bimolecular complex exchanging in intermediate-to-fast NMR time scale, which is a fast dissociating complex. Mapping of CSPs onto the structure showed that dynamin binds to the canonical SH3 binding site in amphiphysin 2 (Fig. 2*B*). The largest CSPs, $\delta\Delta > 0.1$ ppm, were observed for residues Thr-534 and Glu-538 in the RT loop and Asp-559 in the n-Src loop as well as Val-583–Phe-588 in the 3_{10} helix and residues flanking it. All residues showing significant CSPs were located on the rims of the canonical hydrophobic peptide binding groove.

The binding epitope in dynamin was characterized by analyzing CSP and NOE data from a sample containing ^{13}C,^{15}N-labeled dynamin saturated with a 7-fold excess of unlabeled amp-SH3. Chemical shift assignment of dynamin in amp-SH3-bound form turned out to be a non-straightforward process due to line-broadening caused by intermediate exchange as well as multiple conformations observed for residues outside the binding epitope (Fig. 2*C*). Intermolecular NOEs between dynamin residues ^{830}PQVP^{833} and aromatic residues in amp-SH3 were observed, these aromatic residues most probably corresponding to Trp-562 and Phe-588 in the canonical hydrophobic binding pockets (explicit NOE peak assignment was not performed). No unambiguous intermolecular NOEs were observed outside the tetrapeptide. However, the proton resonances of Arg-835 were significantly up-field-shifted, presumably due to the proximity of amp-SH3 Trp-562. Additionally, for residues 831–838 a single set of peaks was observed in the ^{1}H,^{15}N HSQC spectrum whereas for residues at peptide termini, 820–827 and

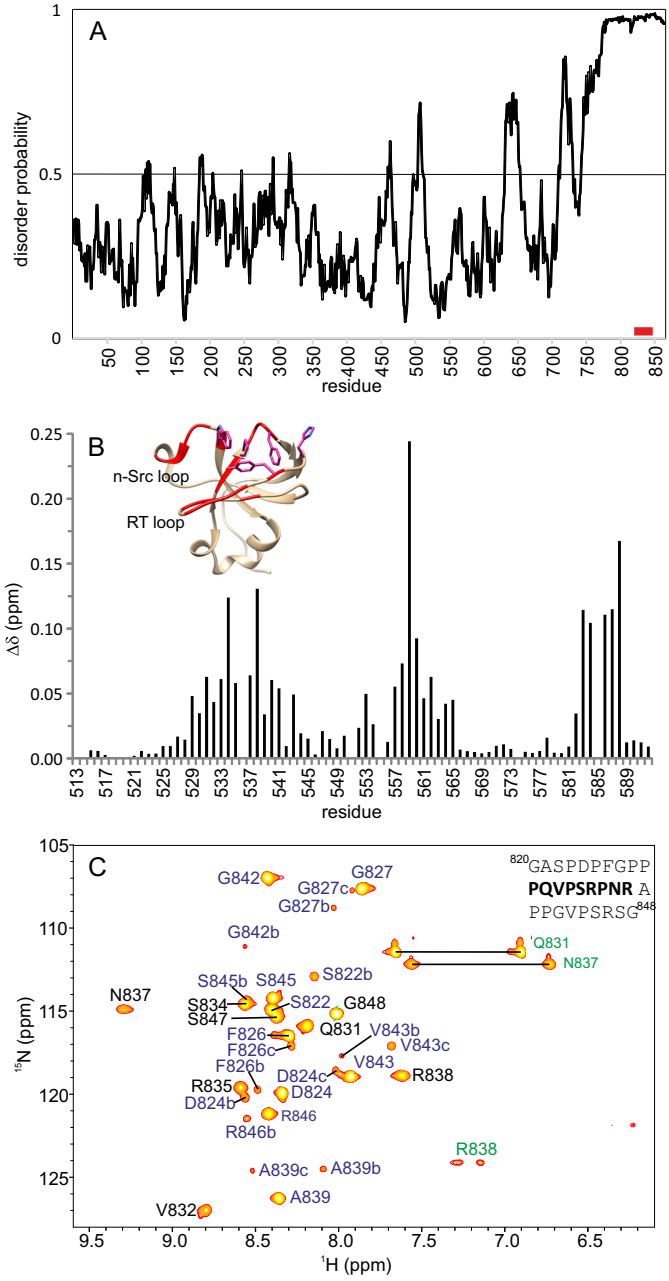

FIGURE 2. **Dynamin and its interaction with amp-SH3.** *A*, IUPred disorder prediction (17) for dynamin. Scores above 0.5 indicate disorder. Location of the 29-mer peptide of dynamin used in the study is indicated with a *red line*. *B*, per residue chemical shift perturbations observed for amp-SH3 when interacting with dynamin C-terminal peptide (residues 820–848). Residues with $\Delta\delta \geq 0.06$ ppm are mapped onto the structure of free amp-SH3 (PDB code 1MUZ; Ref. 16). Residues in the canonical hydrophobic ligand binding interface are highlighted on the free amp-SH3 structure. *C*, $^{1}H,^{15}N$ HSQC spectrum of dynamin peptide when in complex with amp-SH3. Cross-peaks labeled in *black* originate from amide groups, which exist predominantly in a single conformation, whereas peaks labeled in *blue* originate from amide groups in multiple conformations. Side-chain cross-peaks are labeled in *green*. The peptide sequence is given in the *upper right corner* with the binding epitope in *bold*.

839–848, two or three sets of peaks were present (Fig. 2*C*). These results suggest that amp-SH3 recognizes ^{830}PQVPSRPNR^{838} as the binding epitope in dynamin. This corresponds to a P*XX*P*X*RP*X*R consensus sequence, where prolines 1 and 4 establish the classical P*XX*P motif. The C-terminal RP*X*R tetra-

TABLE 1

Amp-SH3 binding thermodynamics measured using ITC

For clarity, peptide sequence alignments are shown below the table. Locations of mutations are highlighted in blue.

amp-SH3 ligand	ΔG (kJ/mol)	ΔH (kJ/mol)	−TΔS (kJ/mol)	K_d (μM)	n
dynamin 820-848*	-28.8	-76.5	47.7	8.90	0.74
dynamin 827-842	-27.3±0.6	-51.5±0.1	24.2±0.6	20.10±0.10	1.06
dynamin 827-842, S834P	-30.7±0.2	-45.8±0.1	15.1±0.3	4.10±0.01	1.07
dynamin 827-842, S834P/N837R	-34.3±0.2	-38.1±0.4	3.8±0.4	0.97±0.01	1.13
SOS1	-30.9±0.2	-40.6±1.5	9.7±1.7	3.90±0.40	1.06
SOS1 P1157R/E1158G	-40.9±0.1	-54.3±0.4	13.4±0.3	0.07±0.00	1.01
CHIKV*	-43.6	-50.4	6.8	0.02	0.97
CHIKV A1733R	-42.7±0.3	-44.8±1.2	2.1±0.9	0.03±0.00	1.13
CHIKV R1739A	-38.0±0.1	-48.6±0.2	10.6±0.3	0.22±0.01	1.03
CHIKV R1739A/R1741S	-37.0±0.4	-47.5±0.8	10.5±1.3	0.33±0.05	1.17
CHIKV R1741S	-42.6±0.8	-57.1±0.6	14.6±0.5	0.04±0.00	1.03
RIN3	-45.5±0.8	-40.4±0.4	-5.2±0.4	0.01±0.00	1.07
SFV	-38.7±0.0	-73.0±0.8	34.3±0.8	0.16±0.01	1.05

```
                                  ***o*o**oo++++-----*oo**o****[1]
>dynamin, long      820GASPDPFGPPPQVPSRPNRAPPGVPSRSG848
>dynamin, short           827GPPPQVPSRPNRAPPG842
>dynamin, S834P           827GPPPQVPPRPNRAPPG842
>dynamin, S834P/N837R     827GPPPQVPPRPRRAPPG842
>SOS1                1144EVPVPPPVPPRRRPESAPAE1163
>SOS1 P1157R/E1158G  1144EVPVPPPVPPRRRRGSAPAE1163
>CHIKV                 1728STVPVAPPRRRRGRNLT1744
>CHIKV A1733R          1728STVPVRPPRRRRGRNLT1744
>CHIKV R1739P/G1740E   1728STVPVAPPRRRPERNLT1744
>CHIKV R1739A          1728STVPVAPPRRRAGRNLT1744
>CHIKV R1739A/R1741S   1728STVPVAPPRRRAGSNLT1744
>CHIKV R1741S          1728STVPVAPPRRRRGSNLT1744
>RIN3                   378KQPPVPPPRKKRISRQL394
>SFV                   1733LENPIPPPRPKRAAYLA1750
```

[1] A minus sign signifies one conformation present for dynamin in the dynamin·amp-SH3 complex. For residues marked with an asterisk more than one conformation for dynamin is present in the complex, and prolines, for which no peaks were observed in the $^{1}H,^{15}N$ HSQC, are marked with the letter o. A plus sign signifies that intermolecular NOEs were observed between these residues and amp-SH3.

peptide element targets the specificity zone of amp-SH3, most probably through an interaction similar to that described below for the amp-SH3·CHIKV complex. Thus, we propose that amp-SH3 recognizes P*XX*P*X*R(P)*X*R-type ligands that harbor the P*X*RP*X*R consensus motif identified earlier (15, 16). Binding thermodynamics was obtained using ITC (Table 1 and Fig. 3*A*). In agreement with the results obtained using NMR spectroscopy, dynamin binds amp-SH3 with relatively low affinity, the dissociation constant (K_d 8.9 μM). The binding is driven by strong negative enthalpy ($\Delta H = -76.5$ kJ/mol), which is counterbalanced by a large entropic penalty ($-T\Delta S = 47.7$ kJ/mol).

C-terminal Tails of CHIKV and SFV nsP3 Are Disordered and Bind amp-SH3 with High Affinity—Disorder prediction using the IUPred algorithm (17) shows that the nsP3 proteins of several alphaviruses, including CHIKV and SFV, have a tendency for disorder in the C-terminal portion (Fig. 4*A*). We sought to understand on the structural level how these viruses recruit amphiphysin-2 to alphaviral replication complexes. To this end, peptides from CHIKV nsP3 (^{1728}STVP**VAPPR**RRRGRNLT^{1744}, with the Class II consensus sequence in bold) and SFV nsP3 (^{1733}LEN**PIPPPR**PKRAAYLA^{1750}) as well as the related peptide from NS5A of HCV subtype 1a (^{2320}RSP**PVPPPR**KRRTVVLT^{2336}) were titrated into ^{15}N-labeled amp-SH3, and binding-induced CSPs were monitored in $^{1}H,^{15}N$ HSQC spectra. The three peptides induced the same type of changes in the spectra: with increasing peptide concentration, peaks of the

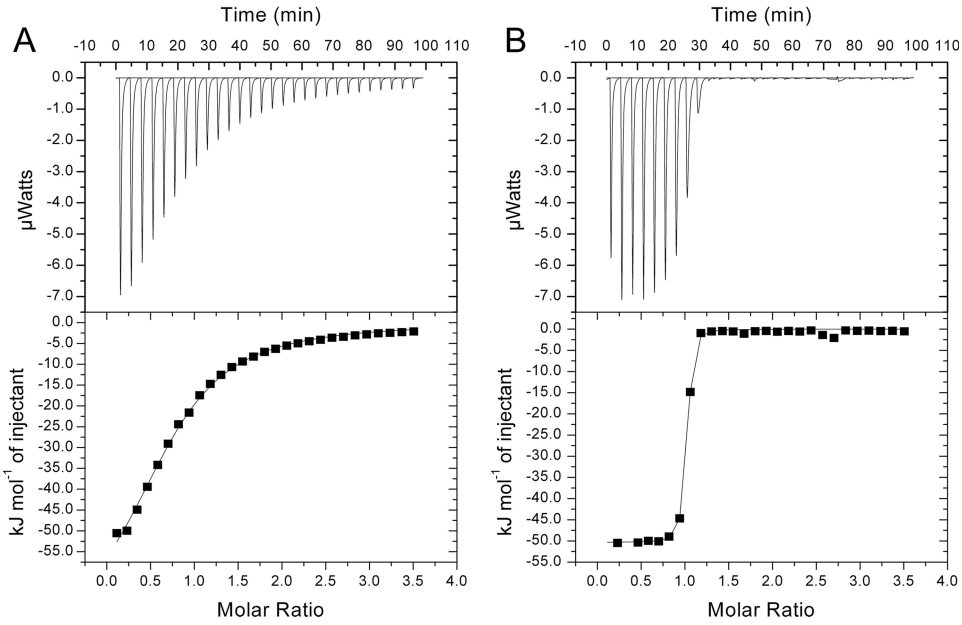

FIGURE 3. **ITC data of amp-SH3.** *A*, interaction of amp-SH3 with dynamin (residues 820–848). *B*, interaction of amp-SH3 with CHIKV nsP3 (residues 1728–1744). The *upper panels* represent raw data, and the *lower panels* represent the binding isotherms.

free form of amp-SH3 disappeared while those of the bound form simultaneously appeared (Fig. 4*B*). This indicates slow complex dissociation in the NMR time scale associated with high affinity binding. Moreover, all three peptides were found to occupy the same binding site given that ligand-induced CSPs were observed for the same residues in amp-SH3 (Fig. 4*B*). Further analysis of CHIKV nsP3 binding using ITC (Table 1 and Fig. 3*B*) showed that the affinity of this viral peptide to amp-SH3 is unusually high, with a K_d of 0.024 μM, clearly among the strongest found for SH3 domains (18). amp-SH3 interacts with SFV nsP3 with an almost 10-fold lower but, nevertheless, high affinity (K_d 0.16 μM). We did not carry out ITC measurements for the HCV NS5A peptide, but based on the slow exchange kinetics observed in NMR titration and its highly similar amino acid composition with CHIKV and SFV, we presume that it also has a similar high amp-SH3 binding affinity. Indeed, a slowly dissociating complex in NMR-based titration experiments and a K_d of 0.24 μM for the subtype 1b peptide of HCV NS5A (^{347}TKAP**PIPPPR**RKRTV^{361}) and amp-SH3 have recently been reported (19).

amp-SH3 in Complex with CHIKV nsP3 Reveals a Canonical Class II Ligand Binding Mode with a Structurally Dispersed Affinity-determining Interaction—To investigate on the structural determinants leading to the very high affinity, we determined the structure of amp-SH3 in complex with CHIKV nsP3 peptide using solution state NMR. Rather than resorting to differently labeled components of the complex and isotope-filtered spectroscopy, we mixed uniformly ^{13}C,^{15}N-labeled CHIKV nsP3 and amp-SH3 in 1:1 concentration ratio and measured a conventional set of triple-resonance experiments as well as ^{15}N- and ^{13}C-edited NOESY experiments for the assignment of amp-SH3 and CHIKV nsP3 resonances and collection of intra- and intermolecular distance restraints. The solution structure of the amp-SH3·CHIKV complex is presented in Fig. 5*A*. The 20 lowest energy structures overlay well, the backbone (N, Cα, C′) and heavy atom r.m.s.d. being 0.36 and 0.74 Å, respectively, for the structured regions of the protein (residues 516–593) and peptide (1730–1736) (Table 2). amp-SH3 adopts the typical SH3 domain-fold consisting of five β strands, connected by the RT loop between β1 and β2, the n-Src loop between β2 and β3, and the distal loop between β3 and β4. A short helical stretch connects β4 to β5. The structure of amp-SH3 in complex with CHIKV is very similar to that of its free form (PDB code 1MUZ; Ref. 16). Structural differences are observed at the peptide binding interface where the side chains of Asp-559, Trp-562, and Phe-588, in direct contact with the peptide in the complex, reposition for optimal interaction. Also, side chains in the cluster of negatively charged residues Asp-535, Asp-537, and Glu-538 in the RT loop and Glu-556 and Glu-557 in the n-Src loop are reoriented to better face the C-terminal arginines of the CHIKV peptide. Side-chain dispersion of residues in the negatively charged cluster is much higher in the complex form, mirroring the conformational heterogeneity of the peptide arginine side chains.

With the exception of Pro-1731 ψ, residues in the structured part of CHIKV peptide in the complex adopt ϕ/ψ angles close to those typically observed in a left-handed PPII conformation (−75/+145°). The ^{1730}VPVAPPR^{1736} binding motif interacts with amp-SH3 in the canonical manner with ^{1730}VP^{1731} and ^{1733}AP^{1734} interacts with the two hydrophobic *X*P grooves formed by the conserved residues His-529, Phe-588, Tyr-531, Trp-562, and Pro-585 (Fig. 5*B*). Backbone atoms of R1736 are relatively well defined in the complex structure, but the structural dispersion increases toward the end of the side chain. Several intermolecular NOE correlations were observed between Arg-1736 and amp-SH3 Asp-559 and Trp-562 side-chain protons. Chemical shifts of Arg-1736 were significantly up-field-shifted, consistent with the arginine side chain being steadily proximal to Trp-562. An averaged guanido signal was, however, observed for Arg-1736, interpreted as conformational

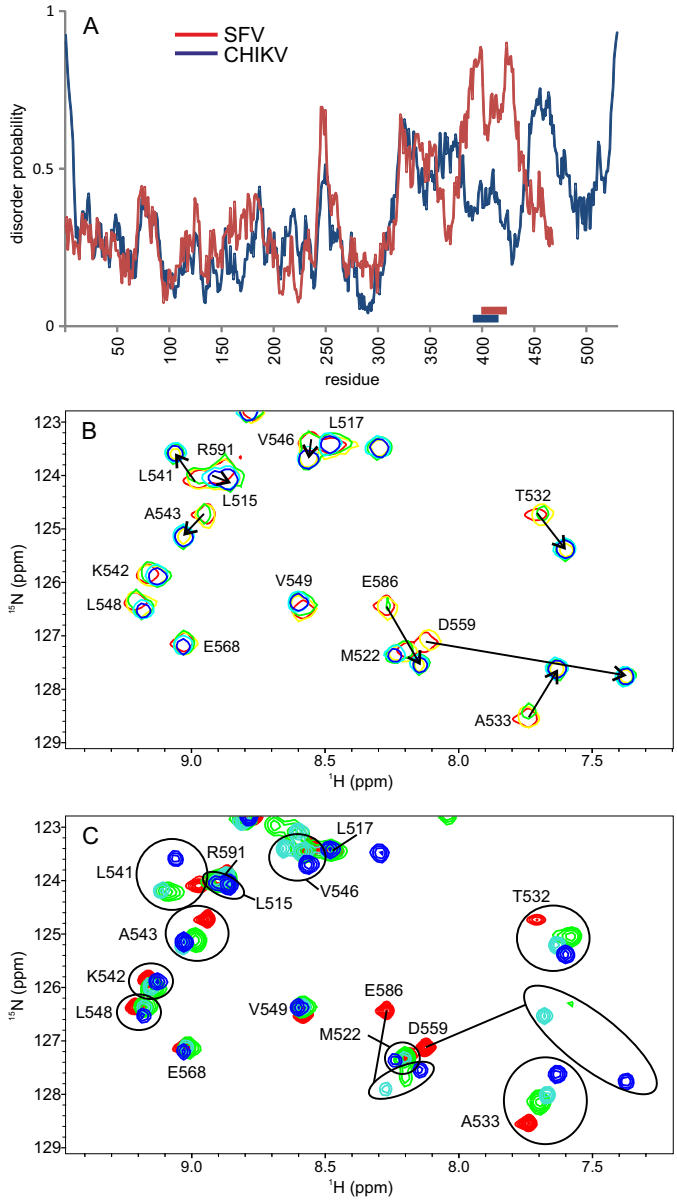

FIGURE 4. ***Alphavirus* peptides and their interaction with amp-SH3.** *A*, IUPred disorder prediction (17) for CHIKV and SFV nsP3. For simplicity, sequence numbering starts from one for both viral proteins. Fragments (nsP3 proteins) shown in the graph correspond to residues 1334–1864 and 1337–1804 for CHIKV and SFV, respectively. Locations of the CHIKV and SFV peptides used in the study are indicated with *lines*. *B*, amp-SH3 binds HCV, SVF, and CHIKV peptides with high affinity, here demonstrated with SVF; a section of an overlay of ^{1}H,^{15}N HSQC spectra of amp-SH3 and SFV with concentration ratios of 1:0 (amp-SH3 to SFV, *red*), 1:0.25 (*yellow*), 1:0.5 (*green*), 1:0.75 (*cyan*), and 1:1 (*blue*) is shown. A slow exchange pattern is observed with peaks disappearing from their position in the ligand-free state and reappearing at their ligand-bound position. *C*, the three peptides induce chemical shift changes for the same residues in amp-SH3. Cross-peaks of the ligand-free form of amp-SH3 are shown in *red*, and those of HCV-, SFV- and CHIKV-bound form (1:1 concentration ratio) are in *cyan*, *blue*, and *green*, respectively.

exchange at the very end of the side chain. Structural dispersion rapidly grew from Arg-1736 toward the C terminus of the peptide. Some structural preference, however, still persisted in ^{1737}RRR^{1739}. Side-chain conformations of Arg-1737 and Arg-1739 were not completely random. Arg-1737 was oriented toward Asp-559 and Glu-560 in the n-Src loop, and Arg-1739 was oriented toward Asp-537, Glu-556, and Glu-557, structurally between the RT and n-Src loops (see supplemental Fig. S2 for the structural representation of the latter interaction). Due to signal overlap and low intensity, NOE peak assignments between these residues were ambiguous, but the tendency for structural order was supported by non-random coil Cα, Cβ, and Hα and non-degenerate Hβ arginine chemical shifts as well as relaxation data (next subsection). Broad ϵ signals were observed for ^{1737}RRR^{1739}. It appears that the ligand arginine side-chain interactions with the SH3 domain surface are transient or fluctuating. Restrictions in the disposable conformational space and, by implication, the preference for alike orientation as well as restricted backbone dynamics could at least partly be caused by like-charge repulsion of successive arginine side chains. For peptide residues C-terminal to Arg-1739, sparse intraresidual and sequential NOE peaks were observed resulting in random conformations with no contact to the protein.

Positively Charged C-terminal Residues in CHIKV Show Restricted Mobility—To attain a more profound knowledge on the rigidity of CHIKV nsP3 in complex with amp-SH3, we measured ^{15}N spin relaxation times as well as heteronuclear {^{1}H}^{15}N NOEs that provide dynamical information on polypeptide backbone in ps-ns time scales (20). Fig. 6 shows residue-specific T_2 relaxation times and heteronuclear NOEs. Similar T_2 and heteronuclear NOE values were observed for the SH3 domain and the region comprising the amp-SH3 binding epitope in nsP3, ^{1731}PVAPPR^{1736}, indicating rigidity on ps-ns time scales also for the peptide binding epitope. T_2 data also reveal that in addition to the consensus binding motif, backbone amides of residues ^{1737}RRR^{1739} are rigid in the ps-ns time scale, whereas residues C-terminal to Arg-1739 show higher T_2 times, indicative of increased backbone dynamics in ps-ns time scale. A similar trend for backbone dynamics was observed in heteronuclear NOEs for the ^{1737}RRR^{1739} epitope outside the canonical class II consensus, although these values are on average slightly lower than those of the SH3 domain. Interestingly, in contrast to the T_2 data, Arg-1741 highlights a relatively high {^{1}H}^{15}N NOE value, suggesting restricted motion in ps-ns time scales.

Fine Mapping of Residues in Cellular and Viral Ligands That Critically Contribute to amp-SH3 Binding—To further characterize the amp-SH3 ligand binding epitope and especially the importance of the multiple arginines in the ligand, we made several mutations to CHIKV nsP3 as well as to its cellular ligand dynamin and measured peptide binding thermodynamics using ITC. A peptide from Son of Sevenless (SOS1), a classic and extensively characterized Class II SH3 ligand, was used as a reference. Amphiphysin-2 has in fact originally been independently discovered through its interaction with the proline-rich region of SOS1 in a yeast two-hybrid screen (21). Sequence alignment of several *Alphavirus* nsP3 proteins together with the sequentially related HCV NS5A suggests a consensus sequence P(I/V)(A/P)PPR(R/K/P)(R/K)(R/K) for viral high affinity amphiphysin ligands (Fig. 1). Dynamin exhibits a similar binding epitope, except that serine replaced proline as the fifth residue (Ser-834 according to dynamin numbering) and asparagine replaced the positively charged R/K as the eighth residue (Asn-836) (Fig. 1 and Table 1). Interestingly, the amino

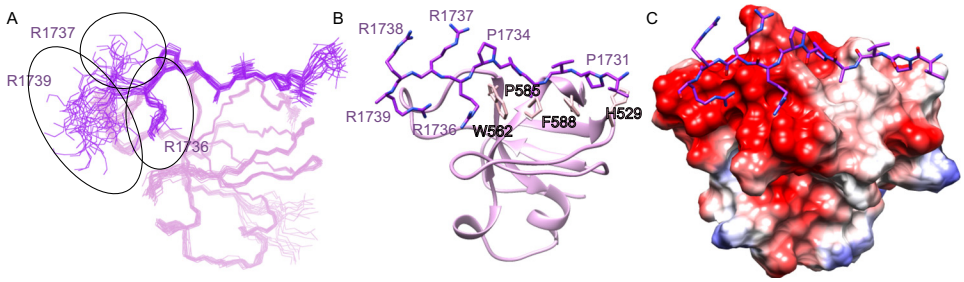

FIGURE 5. **Solution structure of the amp-SH3·CHIKV complex.** *A*, Ensemble of 20 lowest-energy structures. Disordered residues Ser-1728–The-1729, Gly-1740–Thr-1744 of CHIKV, and the side chain of Arg-1738 have been left out for clarity. *B*, the lowest energy structure of the amp-SH3·CHIKV complex with amp-SH3 is show in ribbon, and CHIKV is shown with all heavy atoms. Key residues in the complex interaction are marked on both molecules. *C*, coulombic surface representation of SH3 highlighting the large patch of negative electrostatic potential and the CHIKV peptide interactions with it. The lowest energy structure of the complex is shown. The figures were made with the program UCSF Chimera (39).

TABLE 2
Structural statistics of the amp-SH3·CHIKV complex

Completeness of resonance assignments[a]	
Backbone	99.7%
Side chain, aliphatic	98.0%
Side chain, aromatic	97.0%
Experimental restraints	
Distance restraints	
Total	2,594
Intraresidual ($i = j$)	474
Sequential ($i - j = 1$)	629
Medium range ($1<i - j<5$)	337
Long range ($i-j \geq 5$)	1,154
Intermolecular	153
Dihedral angle restraints	113
No. of restraints per restrained residue	26.7
No. of long range restraints per restrained residue	11.9
Residual restraints violations	
Average no. of distance violations per structure	
0.1–0.2 Å	1.6
0.2–0.5 Å	0 (max. 0.14 Å)
>0.5 Å	0
Model quality[b]	
r.m.s.d. backbone atoms (Å)	0.36
r.m.s.d. heavy atoms (Å)	0.74
r.m.s.d. bond lengths (Å)	0.013
r.m.s.d. bond angles (°)	2.1
Molprobity Ramachandran statistics[b]	
Most favoured regions (%)	96.7
Allowed regions (%)	3.1
Disallowed regions (%)	0.2
Global quality scores (raw/Z score)[b]	
Verify3D	0.33/−2.09
ProsaII	0.61/−0.17
PROCHECK(ϕ-ψ)	−0.39/−1.22
PROCHECK (all)	−0.36/−2.13
Molprobity clash score	5.86/0.52
Model contents	
Ordered residues	516–593, 1730–1736
Total no. of residues	98
BMRB accession number	30,010
PDB ID code	5,I22

[a] Backbone includes Cα, Cβ, N, and H atoms, except the N-terminal amide. For side chains, excluded are the highly exchangeable groups (Lys amino, Arg guanido, Ser/Thr/Tyr hydroxyl, His δ1/ϵ2) as well as all non-protonated carbons and nitrogens.
[b] Ordered residues.

acid sequence of SOS1 is even more similar to the viral consensus with a proline instead of (R/K) as the last residue.

Our results, presented in Table 1, indicate that the wild type, 16-mer dynamin peptide binds amp-SH3 with 3 orders of magnitude lower affinity than the CHIKV nsP3 peptide (~20 *versus* 0.02 μM) and that despite its high sequence similarity with CHIKV nsP3, the SOS1 peptide binds amp-SH3 with an affinity comparable with that of dynamin ($K_d \sim 4$ μM).

We then investigated the role of the P*X*RP*X*R epitope of dynamin (PSRPNR) in amphiphysin binding. We designed substitutions to dynamin aiming to make its amp-SH3 binding motif more viral-like and to possibly improve its binding affinity accordingly. Indeed, a S834P substitution in dynamin (yielding the P*XX*PPR*XX*R consensus) increased amp-SH3 binding affinity significantly (K_d 20.1 μM *versus* 4.1 μM), whereas introduction of a double substitution S834P/N837R (the P*XX*P-PR*X*RR consensus) enhanced dynamin binding further to the high nanomolar range (K_d 0.97 μM). Thermodynamic profiles of dynamin interactions highlight a decrease in the unfavorable entropy contribution to the Gibbs free energy of binding, which overcomes the decrease in binding enthalpy, resulting in a 20-fold increase in binding affinity.

Next, we sought to investigate the role of the C-terminal arginines on the high affinity CHIKV nsP3 amp-SH3 binding. We made mutations to the C-terminal end of the binding epitope; that is, by replacing Arg-1739 with alanine. This resulted in a substantial 10-fold decrease in binding affinity (K_d 0.02 *versus* 0.22 μM). Replacement of ^{1157}PE^{1158} with ^{1157}RG^{1158} in SOS1, which renders SOS1 CHIKV-like, resulted in a dramatic 55-fold increase in binding affinity (K_d 3.90 μM *versus* K_d 0.07 μM). The role of Arg-1741 is tangential at most, as deduced from the faint effects on K_d the mutation of this residue produces. This is in accord with the complex structure in which this arginine does not interact with amp-SH3 surface. It might, however, have a role in constraining the available space of the Arg-1739 side chain through side-chain repulsive effects.

Finally, ITC data reveals the role of basic residue (R/K) with respect to proline at position 7 in P*XX*PPR(**R**/**K**/**P**)(R/K)(R/K) consensus. Some viral ligands, including SVF nsP3, have proline at position 7, whereas some viral nsP3s *e.g.* CHIKV and the related HCV NS5A, have either Arg or Lys at this position. A thermodynamic profile shows a large entropic penalty for SVF ($-T\Delta S = 34.3$ kJ/mol) compared with that of CHIKV ($-T\Delta S =$ 6.8 kJ/mol). This underpins the favorable contribution of a basic residue at position 7 to overall binding affinity (SFV $K_d =$ 0.16 μM *versus* CHIKV $K_d = 0.024$ μM). Interestingly, dynamin and many other cellular ligands of amp-SH3 also harbor a proline at position 7, and its thermodynamic signature displays a large entropic penalty ($-T\Delta S = 47.7$ kJ/mol) to Gibbs free energy of binding. With respect to proline at position 7, SFV nsP3 resembles more than CHIKV nsP3, the cellular ligands.

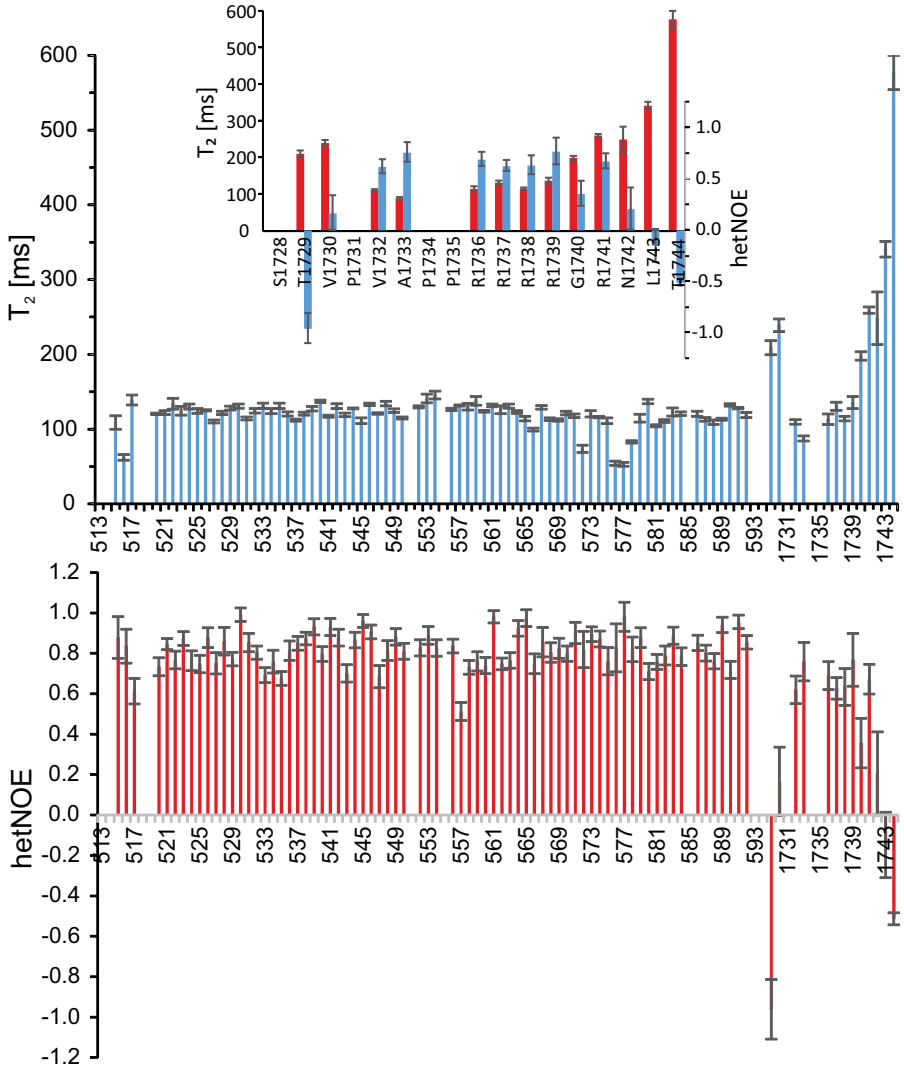

FIGURE 6. **amp-SH3·CHIKV complex dynamics.** Residue specific T_2 relaxation times and heteronuclear NOEs are shown for amp-SH3 (residues 513–593) and CHIKV (1728–1744). An expansion of the peptide data is given in the *inset*.

This implies a significant role for the positively charged C-terminal residues in amp-SH3 binding despite the side-chain structural dispersion observed in the complex structure. The results of site-directed mutations assessed with ITC are well in line with the ^{15}N relaxation data, which shows restricted ps-ns time-scale backbone motion for the C-terminal arginine residues in CHIKV (Fig. 6).

Human High Affinity amp-SH3 Binding Motif Matching the Viral Consensus—Intrigued by the apparent binding motif dissimilarities and the associated large differences in affinity for amp-SH3 that typified the viral *versus* the cellular amphiphysin ligands, we carried out an bioinformatics search of the human proteome (Prosite in ExPASy) using the amino acid string P(I/V)(A/P)PPR*X*(R/K)(R/K) to see if any viral-like amp-SH3 binding motifs could be found. This query produced two hits. The linear motif PIPPPRLKK was found to be present in the second proline-rich domain (PRD) of RIN2 (Ras and Rab interactor 2), and PVPPPRKRR found in the third PRD of RIN3 (22). Interestingly, we noticed that a capacity to bind amphiphysin in an SH3-dependent manner had in fact already been documented for both RIN2 and RIN3 (23). We thus performed ITC measurements with a 17-mer RIN3 peptide ^{378}KQP**PVPPPRKKR**IS-RQL^{394} containing the linear motif matching the viral consensus motif. In agreement with our predictions, but yet strikingly, this RIN3 peptide bound amp-SH3 with a remarkably low K_d value of 10 nM (Table 1), which to our knowledge is the strongest affinity measured for any natural SH3 binding ligand found to date.

Discussion

We have solved the three-dimensional solution NMR structure of amphiphysin-2 SH3 domain in complex with CHIKV nsP3 peptide spanning residues 1728–1744. In addition, we have characterized the binding thermodynamics of several cellular and viral amp-SH3 targeting peptides and mapped residues vital to high affinity amp-SH3 binding using ITC.

Our results indicate that dynamin, a well characterized natural ligand of amp-SH3 binds in class II orientation with low micromolar affinity and that viral peptides from SFV, CHIKV, and HCV use the same binding site on the surface of amp-SH3 with the same orientation but show remarkably higher affinity. Positively charged residues within and after the P(V/I)(A/

P)PPR*X*(R/K)(R/K) consensus sequence are vital for this tight binding. The five C-terminal arginines present in CHIKV nsP3 translate into a nanomolar affinity to amp-SH3. Our ITC data (Table 1) indicate significant contributions to the binding affinity even from the two most distant arginines, Arg-1739 and Arg-1741, despite the fact that CHIKV nsP3 arginines do not have a definite conformation but instead possess increasing mobility toward the end of their side chain and toward the C terminus of the peptide.

The pivotal role of the basic residues ensues from the unique surface charge distribution on amp-SH3. Negatively charged residues from the RT and n-Src loops form a large surface next to the canonical hydrophobic peptide binding interface with which the basic residues interact. Comparison of the structures and binding affinities of amp-SH3 in complex with CHIKV *versus* the adaptor CD2-associated protein (CD2AP) SH3–2 in complex with RIN3ϵ2 (PDB code 3U23; Ref. 24) emphasizes the need for matching counterparts in the portrayed electrostatic interaction. RIN3ϵ2 can be seen to adopt a polyproline II helix conformation in class II orientation almost identical to that observed for nsP3 in the amp-SH3·CHIKV complex. Moreover, the structural match of the conserved residues on the two SH3 domains is nearly perfect (supplemental Fig. S1). Interestingly, the basic residues Arg-462–Lys-463–Lys-464 in RIN3ϵ2 equivalent to Arg-1736–Arg-1737–Arg-1738 in CHIKV show two side-chain conformations in the crystal structure, reminiscent of the disorder observed in CHIKV. The classical binding interactions being alike, the 200-fold difference in binding affinity between RIN3ϵ2 and CD2AP (2.1 μM, (24) compared with that between RIN3 and amp-SH3 (0.01 μM, Table 1) primarily originates from the difference in the surface electrostatic potential of the two SH3 domains. Indeed, the surface charge distribution is different in the two SH3 domains (supplemental Fig. S1). Due to amp-SH3 side chain dynamics, the exact shape of the negatively charged surface of amp-SH3 varies between structures in the ensemble but is invariably larger than that observed in CD2AP SH3–2. The larger size is the result of a five-residue longer acidic n-Src loop, which extends the negatively charged surface in amp-SH3 parallel to the direction of the peptide backbone. This surface can accommodate interactions with all four arginine guanido groups in CHIKV as compared with two Arg/Lys in RIN3 within a hydrogen-bond distance from acidic residues on CD2AP SH3–2.

This interaction between basic residues and a negatively charged surface patch bears a resemblance to the "polyelectrostatic interaction" described for the dynamic complex between Sic1, an intrinsically disordered, highly charged protein with multiple phosphorylation sites (termed CPDs), and Cdc4, a globular protein with a single CPD binding site (25, 26). The polyelectrostatic effect arises from the joint energy contributions from specific interactions within the binding site and nonspecific, long range electrostatic interactions between the binding partners. The latter are depicted as a mean electrostatic field created by charged, rapidly interconverting conformers of the disordered region. A cumulative effect of all charges in the disordered ligand is anticipated in this interaction model.

The best known cellular ligands of amphiphysin, namely dynamin and synaptojanin 1, as well as c-Myc (with one mismatch) share similar proline-rich amphiphysin target sequences (Fig. 1). They all use a P*XX*P*X*Rp*X*R motif for binding to amp-SH3, but unlike viral amphiphysin ligands, they are not enriched in basic residues between the two conserved arginines. In Semliki forest, Barmah forest, Mayaro, and Aura viruses nsP3s these "P*X*" consensus residues are PK, whereas in CHIKV nsP3 and HCV NS5A they are RR and RK, respectively. As shown, these additional basic residues are the origin of the high affinity of these viral ligands, thereby enabling them to usurp host cell amphiphysin to promote virus replication. Alphaviral nsP3 takeover of amphiphysin, mediated through the SH3 domain, robustly facilitates viral RNA replication. The exact function of amphiphysin in viral replication is unclear, but a role in formation or stabilization of the membranous replication structures by means of the BAR ((BIN/amphiphysin/Rvs) domain has been envisaged (9). Moreover, the interaction between HCV NS5A and amphiphysin can contribute to a favorable environment for productive viral replication by inhibiting Bin1-mediated apoptosis (27), possibly due to competitively blocking the binding of Myc to Bin1 (19).

Mimicry of host protein SLiMs is a common pathogen stratagem to manipulate host cell functions (3, 28). SLiMs have been defined as short stretches of contiguous amino acids typically residing in intrinsically disordered protein segments. The small size of SLiMs limits binding to few intermolecular contacts, resulting in low affinity complexes characterized by fast on and off rates integral in *e.g.* regulatory processes. These motifs are susceptible to competition by higher affinity viral mimics. In the case of SH3 domains, as shown in this study, expansion of intermolecular contacts outside the classical P*XX*P consensus region has proven to be an efficient mechanism to increase affinity.

Interestingly, although fulfilling the same general goal, the underlying hijacking mechanism employed by CHIKV is completely different from that of the effector $EspF_U$ from the pathogenic strain 0157:H7 of enterohemorrhagic *Escherichia coli* (29, 30). The latter utilizes a W switch to increase its avidity to IRTKS SH3 by enhancing enthalpic contribution, at the expense of favorable entropy, to the largely hydrophobic interaction between IRTKS SH3 and $EspF_U$. In combination with a relatively large linear binding epitope targeting the specificity zone of IRKTS SH3, the W switch warrants a high nanomolar range affinity, enabling capture of the host's actin polymerization machinery. CHIKV has chosen a different strategy; affinity is increased through a polyelectrostatic interaction between positively charged arginines of nsP3 and a negatively charged specificity zone of amp-SH3. The partially disordered state of nsP3 arginines offers a large binding epitope while minimizing entropic penalty upon binding to amp-SH3.

With its extreme affinity for amp-SH3, RIN3 stands out among the known cellular amphiphysin ligands. In agreement with this high binding affinity, it has been shown that co-expression of BIN1/amphiphysin-2 with RIN3 in HeLa cells leads to a prominent SH3-dependent relocalization of otherwise diffusively cytoplasmic BIN1 into RIN3-positive endocytic vesicles (23). Recruitment of RIN3 itself into these vesicles is triggered by tyrosine phosphorylation-regulated association of RIN3 with a Ras GTPase (31). We speculate that the availability

of the amp-SH3 binding site in RIN3 must also be strictly regulated to avoid permanent association between BIN1 and amphiphysin-2 in cells. Indeed, similar to the majority of other SH3-mediated signaling protein interactions, the typical cellular binding partners of amphiphysin, such as dynamin, have dramatically lower amp-SH3 binding affinities and, unlike the viral ligands, appear to be evolutionary optimized for selectivity as well as capacity for dynamic and plastic modulation rather than maximal affinity. The P*XX*P*X*Rp*X*R consensus amp-SH3 motif lacking additional positively charged side chains, which is characteristic for these cellular ligands, may provide a useful strategy for creating specificity and tunability in these interactions. The extreme affinity the amp-SH3-RIN3 is thus an interesting exception to this norm, which could be a fruitful subject of further investigations. In this regard it is worth noting that it may not be a coincidence that both BIN1 and RIN3 have been identified as susceptibility loci for Alzheimer disease (32).

In summary, we have demonstrated the structural basis of the high affinity between CHIKV nsP3 proline-rich motif and amphiphysin-2 SH3 domain. Based on our data this mode of binding very likely also explains the high binding affinity of the proline-rich peptides from RIN3, SFV nsP3, and HCV NS5A. The essence is the polyelectrostatic interaction between the peptide arginines past the canonical Class II binding epitope and the large negative surface electrostatic potential of the SH3 domain. Our data show the consensus sequences P*XX*P*X*Rp*X*R much better denotes the binding preferences of the amphiphysin SH3 domain than the previously described binding motif P*X*RP*X*R and provide another example of a strategy to build remarkably high affinity SH3 interaction that viruses have evolved to exploit.

Experimental Procedures

Protein Production—The gene encoding the SH3 domain (residues 513–593) of human Amphiphysin-2/BIN1 (UniProt O00499) (amp-SH3) was cloned to pET15b vector (Novagen) into the NcoI and XhoI sites. The gene encoding residues 1728–1744 of the C-terminal tail of CHIKV nsP3 (UniProt Q8JUX6) (CHIKV peptide) and the gene encoding GB1 protein were amplified with PCR and combined by using overlapping PCR technique. Tobacco etch virus protease cleavage site was engineered between GB1 fusion protein and CHIKV, and NdeI and XhoI recognition sites were added to the 5′ and 3′ ends of the constructs, respectively. The resulting DNA product encoding GB1-CHIKV fusion protein was cloned into the pET15b vector into the appropriate cloning site.

Production of ^{15}N- and ^{13}C,^{15}N-labeled amp-SH3 or GB1-CHIKV proteins was carried out by transforming plasmids into the BL21(DE3) cells. Cells were grown in M9 minimal media, supplemented with 1 g/liter $^{15}NH_4Cl$ or with 1 g/liter $^{15}NH_4Cl$ and 2 g/liter D-[^{13}C]glucose as the sole nitrogen or nitrogen and carbon source, respectively. Cell culture was incubated at 37 °C, and temperature was decreased to 16 °C when the optical density (OD) of the cell culture reached 0.4, and protein production was induced with 1 mM isopropyl 1-thio-β-D-galactopyranoside when the OD of the cell culture reached 0.6. Cells were further incubated at 16 °C for 16 h and collected by centrifugation. Unlabeled proteins were produced similarly, except Luria broth was used as a culture medium. Cells were disrupted with sonication, and resulting supernatant was clarified by centrifugation with 30,000 × *g*.

Clarified supernatant of amp-SH3 in buffer containing 50 mM Tris-HCl, pH 8, 1 mM DTT was applied to 5-ml CaptoQ ion exchange column (GE Healthcare) and eluted by increasing NaCl linearly to 1 M. Fractions containing amp-SH3 protein were concentrated by Vivaspin2 (SartoriusStedim) concentrator and subsequently applied into the Superdex30 16/60 gel filtration column (GE Healthcare). Buffer used in gel filtration contained 20 mM sodium phosphate, pH 6.5, and 50 mM NaCl, 1 mM DTT (NMR buffer). Fractions with pure amp-SH3 were pooled and concentrated for NMR studies.

Clarified supernatant of GB1-CHIKV peptide was applied to the 1-ml His GraviTrap column (GE Healthcare) according to the manufacturer's instructions. Eluted proteins were extensively dialyzed against phosphate-buffered saline. The His-tag-GB1 fusion from CHIKV peptide was removed by tobacco etch virus protease digestion. Digestion mixtures were applied to His GraviTrap column. Cleaved CHIKV peptide eluted with the flow-through, which was lyophilized to dryness. Lyophilized CHIKV peptide was dissolved in 0.4 ml of H_2O and applied into the SuperdexPeptide 10/300 GL gel filtration column equilibrated with 0.15 M ammonium bicarbonate. Fractions containing purified proteins were pooled and lyophilized. Lyophilized CHIKV peptide was dissolved in NMR buffer before NMR measurements.

All gel filtrations were performed by using the ÄKTA Purifier FLPC purification system (GE Healthcare). According to the SDS-PAGE and MALDI-TOF mass spectra, neither protein contained degradation products or other protein impurities. The synthetic peptides were obtained from GenScript USA, Inc.

NMR Spectroscopy—NMR spectra were recorded at 25 °C on a Varian Unity INOVA 800 MHz NMR spectrometer. Resonance assignment for the amp-SH3·CHIKV complex was carried out with standard triple resonance experiments: HNCACB, CBCA(CO)NH, C(CCO)NH, H(CCO)NH, HBHA-(CO)NH, and HCCH-COSY. Aromatic side chain resonances were obtained from (HB)CB(CGCD)HD and (HB)CB(CGCD-CE)HE spectra as well as ^{15}N- and ^{13}C-edited NOESY-HSQC spectra. The last two were also used to retrieve interproton distance restraints.

Peptide binding epitopes were studied by NMR titration experiments where each of the peptides (dynamin, CHIKV, HCV, and SFV) was added to free amp-SH3 in steps of 1:0, 1:0.25, 1:0.5, 1:0.75, and 1:1 protein-to-peptide concentration ratios. At each concentration ratio a ^{1}H,^{15}N HSQC spectrum was acquired. Backbone resonance assignment of free amp-SH3 was performed with HNCACB and CBCA(CO)NH spectra. T_2 and heteronuclear steady-state NOE spectra were acquired with standard relaxation experiments. Fast chemical exchange of unprotected amide proton can artificially reduce T_2 times. Its impact accentuates at high sample pH and temperature or in the case of a disordered target protein. New approaches for quantitative data acquisition and interpretation have recently been proposed (33). Although sample conditions used in the study (pH 6.5, 7% D_2O at 25 °C) promote low

exchange, the T_2 data should be interpreted qualitatively in unstructured regions. The recycle delay in $\{^1H\}^{15}N$ NOE spectra was set to 5 s. Chemical exchange with saturated water protons can artificially increase heteronuclear NOE ratios in case the recycle delay is set too short (34). As a control a second set of heteronuclear NOE spectra with a 10 s recycle delay was acquired. Within experimental error, the two data sets produced the same results.

Structure Calculations—Structure calculations, based on automated NOE peak assignments, and ϕ and ψ dihedral angle restraints generated with TALOS (35) from the assigned chemical shifts were performed by using Cyana 2.1 structure calculation package (36). The best 20 Cyana structures were subsequently refined in explicit water with AMBER 14 (37). The protein structure validation software suite PSVS (38) was used for structure quality evaluation and validation.

ITC—ITC experiments were performed at 25 °C using a VP-ITC microcalorimeter (GE Healthcare). Synthetic peptides were dissolved in double distilled H_2O, and pH was adjusted to 6.5 with NaOH, lyophilized, and dissolved in NMR buffer for final concentration of 0.3–0.5 mM. Peptides were titrated separately into the 30 μM amp-SH3 solution in the sample cell. Experiments were repeated twice. To measure heats of dilution, control experiments were performed by titrating peptide to buffer and subtracted from raw titration data. Thermodynamic profiles of the amp-SH3 and peptide interactions were obtained by nonlinear least square fitting of experimental data using a single-site binding model of the Origin 7 software.

Author Contributions—P. P. and K. S. conceived and coordinated the study. O. A., M. H., and P. P. designed, performed, and analyzed the ITC experiments. O. A., H. T., and P. P. designed, performed, and analyzed the NMR experiments. All authors reviewed the results and wrote and approved the final version of the manuscript.

Acknowledgments—We acknowledge CSC-IT Center for Science Ltd., Finland, for the allocation of computational resources. We thank Elina Ahovuo for excellent technical assistance.

References

1. Saksela, K., and Permi, P. (2012) SH3 domain ligand binding: What's the consensus and where's the specificity? *FEBS Lett.* **586,** 2609–2614
2. Diella, F., Haslam, N., Chica, C., Budd, A., Michael, S., Brown, N. P., Trave, G., and Gibson, T. J. (2008) Understanding eukaryotic linear motifs and their role in cell signaling and regulation. *Front. Biosci.* **13,** 6580–6603
3. Davey, N. E., Travé, G., and Gibson, T. J. (2011) How viruses hijack cell regulation. *Trends Biochem. Sci.* **36,** 159–169
4. Prokic, I., Cowling, B. S., and Laporte, J. (2014) Amphiphysin 2 (BIN1) in physiology and diseases. *J. Mol. Med.* **92,** 453–463
5. Mim, C., and Unger, V. M. (2012) Membrane curvature and its generation by BAR proteins. *Trends Biochem. Sci.* **37,** 526–533
6. Shupliakov, O., Löw, P., Grabs, D., Gad, H., Chen, H., David, C., Takei, K., De Camilli, P., and Brodin, L. (1997) Synaptic vesicle endocytosis impaired by disruption of dynamin-SH3 domain interactions. *Science* **276,** 259–263
7. Cestra, G., Castagnoli, L., Dente, L., Minenkova, O., Petrelli, A., Migone, N., Hoffmüller, U., Schneider-Mergener, J., and Cesareni, G. (1999) The SH3 domains of endophilin and amphiphysin bind to the proline-rich region of synaptojanin 1 at distinct sites that display an unconventional binding specificity. *J. Biol. Chem.* **274,** 32001–32007
8. Pineda-Lucena, A., Ho, C. S., Mao, D. Y., Sheng, Y., Laister, R. C., Muhandiram, R., Lu, Y., Seet, B. T., Katz, S., Szyperski, T., Penn, L. Z., and Arrowsmith, C. H. (2005) A structure-based model of the c-Myc/Bin1 protein interaction shows alternative splicing of Bin1 and c-Myc phosphorylation are key binding determinants. *J. Mol. Biol.* **351,** 182–194
9. Neuvonen, M., Kazlauskas, A., Martikainen, M., Hinkkanen, A., Ahola, T., and Saksela, K. (2011) SH3 domain-mediated recruitment of host cell amphiphysins by *Alphavirus* nsP3 promotes viral RNA replication. *PLoS Pathog.* **7,** e1002383
10. Spuul, P., Balistreri, G., Kääriäinen, L., and Ahola, T. (2010) Phosphatidylinositol 3-kinase-, actin-, and microtubule-dependent transport of Semliki Forest Virus replication complexes from the plasma membrane to modified lysosomes. *J. Virol.* **84,** 7543–7557
11. Park, E., and Griffin, D. E. (2009) The nsP3 macro domain is important for Sindbis virus replication in neurons and neurovirulence in mice. *Virology* **388,** 305–314
12. Tuittila, M., and Hinkkanen, A. E. (2003) Amino acid mutations in the replicase protein nsP3 of Semliki Forest virus cumulatively affect neurovirulence. *J. Gen. Virol.* **84,** 1525–1533
13. Zech, B., Kurtenbach, A., Krieger, N., Strand, D., Blencke, S., Morbitzer, M., Salassidis, K., Cotten, M., Wissing, J., Obert, S., Bartenschlager, R., Herget, T., and Daub, H. (2003) Identification and characterization of amphiphysin II as a novel cellular interaction partner of the hepatitis C virus NS5A protein. *J. Gen. Virol.* **84,** 555–560
14. Moradpour, D., Gosert, R., Egger, D., Penin, F., Blum, H. E., and Bienz, K. (2003) Membrane association of hepatitis C virus nonstructural proteins and identification of the membrane alteration that harbors the viral replication complex. *Antiviral Res.* **60,** 103–109
15. Grabs, D., Slepnev, V. I., Songyang, Z., David, C., Lynch, M., Cantley, L. C., and De Camilli, P. (1997) The SH3 domain of amphiphysin binds the proline-rich domain of dynamin at a single site that defines a new SH3 binding consensus sequence. *J. Biol. Chem.* **272,** 13419–13425
16. Owen, D. J., Wigge, P., Vallis, Y., Moore, J. D., Evans, P. R., and McMahon, H. T. (1998) Crystal structure of the amphiphysin-2 SH3 domain and its role in the prevention of dynamin ring formation. *EMBO J.* **17,** 5273–5285
17. Dosztányi, Z., Csizmok, V., Tompa, P., and Simon, I. (2005) IUPred: web server for the prediction of intrinsically unstructured regions of proteins based on estimated energy content. *Bioinformatics* **21,** 3433–3434
18. Li, S. S. (2005) Specificity and versatility of SH3 and other proline-recognition domains: structural basis and implications for cellular signal transduction. *Biochem. J.* **390,** 641–653
19. Aladag, A., Hoffmann, S., Stoldt, M., Bösing, C., Willbold, D., and Schwarten, M. (2014) Hepatitis C virus NS5A is able to competitively displace c-Myc from the Bin1 SH3 domain in vitro. *J. Pept. Sci.* **20,** 334–340
20. Farrow, N. A., Muhandiram, R., Singer, A. U., Pascal, S. M., Kay, C. M., Gish, G., Shoelson, S. E., Pawson, T., Forman-Kay, J. D., and Kay, L. E. (1994) Backbone dynamics of a free and phosphopeptide-complexed Src homology 2 domain studied by 15N NMR relaxation. *Biochemistry* **33,** 5984–6003
21. Leprince, C., Romero, F., Cussac, D., Vayssiere, B., Berger, R., Tavitian, A., and Camonis, J. H. (1997) A new member of the amphiphysin family connecting endocytosis and signal transduction pathways. *J. Biol. Chem.* **272,** 15101–15105
22. Saito, K., Murai, J., Kajiho, H., Kontani, K., Kurosu, H., and Katada, T. (2002) A novel binding protein composed of homophilic tetramer exhibits unique properties for the small GTPase Rab5. *J. Biol. Chem.* **277,** 3412–3418
23. Kajiho, H., Saito, K., Tsujita, K., Kontani, K., Araki, Y., Kurosu, H., and Katada, T. (2003) RIN3: a novel Rab5 GEF interacting with amphiphysin II involved in the early endocytic pathway. *J. Cell Sci.* **116,** 4159–4168
24. Rouka, E., Simister, P. C., Janning, M., Kumbrink, J., Konstantinou, T., Muniz, J. R., Joshi, D., O'Reilly, N., Volkmer, R., Ritter, B., Knapp, S., von Delft, F., Kirsch, K. H., and Feller, S. M. (2015) Differential recognition preferences of the three Src homology 3 (SH3) domains from the adaptor CD2-associated protein (CD2AP) and direct association with Ras and Rab interactor 3 (RIN3). *J. Biol. Chem.* **290,** 25275–25292
25. Borg, M., Mittag, T., Pawson, T., Tyers, M., Forman-Kay, J. D., and Chan, H. S. (2007) Polyelectrostatic interactions of disordered ligands suggest a physical

basis for ultrasensitivity. *Proc. Natl. Acad. Sci. U.S.A.* **104,** 9650–9655
26. Mittag, T., Kay, L. E., and Forman-Kay, J. D. (2010) Protein dynamics and conformational disorder in molecular recognition. *J. Mol. Recognit.* **23,** 105–116
27. Nanda, S. K., Herion, D., and Liang, T. J. (2006) The SH3 binding motif of HCV [corrected] NS5A protein interacts with Bin1 and is important for apoptosis and infectivity. *Gastroenterology* **130,** 794–809
28. Via, A., Uyar, B., Brun, C., and Zanzoni, A. (2015) How pathogens use linear motifs to perturb host cell networks. *Trends Biochem. Sci.* **40,** 36–48
29. Aitio, O., Hellman, M., Kazlauskas, A., Vingadassalom, D. F., Leong, J. M., Saksela, K., and Permi, P. (2010) Recognition of tandem P*XX*P motifs as a unique Src homology 3-binding mode triggers pathogen-driven actin assembly. *Proc. Natl. Acad. Sci. U.S.A.* **107,** 21743–21748
30. Aitio, O., Hellman, M., Skehan, B., Kesti, T., Leong, J. M., Saksela, K., and Permi, P. (2012) Enterohaemorrhagic *Escherichia coli* exploits a tryptophan switch to hijack host f-actin assembly. *Structure* **20,** 1692–1703
31. Yoshikawa, M., Kajiho, H., Sakurai, K., Minoda, T., Nakagawa, S., Kontani, K., and Katada, T. (2008) Tyr-phosphorylation signals translocate RIN3, the small GTPase Rab5-GEF, to early endocytic vesicles. *Biochem. Biophys. Res. Commun.* **372,** 168–172
32. Lambert, J. C., Ibrahim-Verbaas, C. A., Harold, D., Naj, A. C., Sims, R., Bellenguez, C., DeStafano, A. L., Bis, J. C., Beecham, G. W., Grenier-Boley, B., Russo, G., Thorton-Wells, T. A., Jones, N., Smith, A. V., Chouraki, V., *et al.* (2013) Meta-analysis of 74,046 individuals identifies 11 new susceptibility loci for Alzheimer's disease. *Nat. Genet.* **45,** 1452–1458
33. Kim, S., Wu, K.-P., and Baum, J. (2013) Fast hydrogen exchange affects ^{5}N relaxation measurements in intrinsically disordered proteins. *J. Biomol. NMR* **55,** 249–256
34. Renner, C., Schleicher, M., Moroder, L., and Holak, T. A. (2002) Practical aspects of the 2D ^{15}N-[1h]-NOE experiment. *J. Biomol. NMR* **23,** 23–33
35. Shen, Y., Delaglio, F., Cornilescu, G., and Bax, A. (2009) TALOS+: a hybrid method for predicting protein backbone torsion angles from NMR chemical shifts. *J. Biomol. NMR* **44,** 213–223
36. López-Méndez, B., and Güntert, P. (2006) Automated protein structure determination from NMR spectra. *J. Am. Chem. Soc.* **128,** 13112–13122
37. Case, D. A., Cheatham, T. E., 3rd, Darden, T., Gohlke, H., Luo, R., Merz, K. M., Jr., Onufriev, A., Simmerling, C., Wang, B., and Woods, R. J. (2005) The Amber biomolecular simulation programs. *J. Comput. Chem.* **26,** 1668–1688
38. Bhattacharya, A., Tejero, R., and Montelione, G. T. (2007) Evaluating protein structures determined by structural genomics consortia. *Proteins* **66,** 778–795
39. Pettersen, E. F., Goddard, T. D., Huang, C. C., Couch, G. S., Greenblatt, D. M., Meng, E. C., and Ferrin, T. E. (2004) UCSF Chimera–a visualization system for exploratory research and analysis. *J. Comput. Chem.* **25,** 1605–1612

Structural Basis of the High-Affinity Interaction Between the Alphavirus Nonstructural Protein-3 (nsP3) and the SH3 Domain of Amphiphysin-2

Helena Tossavainen, Olli Aitio, Maarit Hellman, Kalle Saksela, and Perttu Permi

Supplemental Data

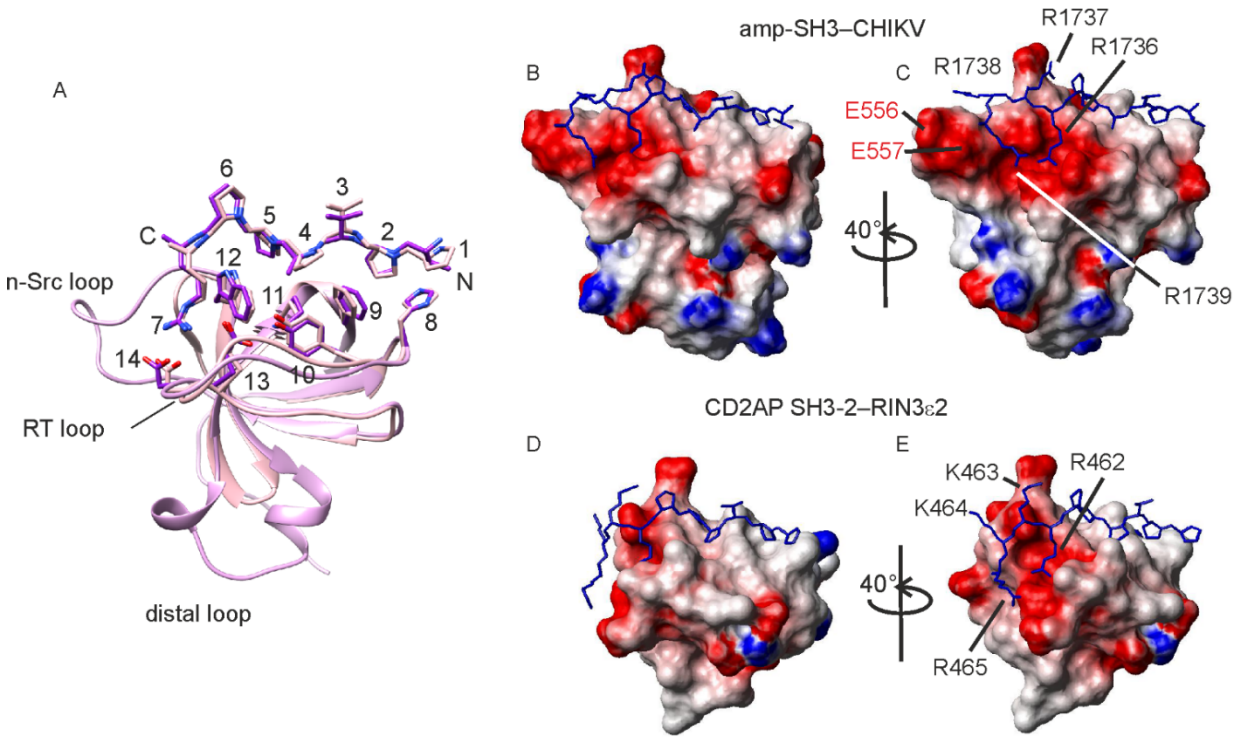

Figure S1. Comparison of amp-SH3 and CD2AP SH3-2 surfaces. *A*, Overlay of amp-SH3–CHIKV (darker colors) and CD2AP SH3-2–RIN3ε2 complexes. Residues involved in the canonical binding interaction are shown in stick model with the following tags: 1, V1730/P456 (CHIKV/RIN3); 2, P1731/457; 3, V1732/458; 4, A1733/P458; 5, P1734/459; 6, P1735/460; 7, R1736/461 and 8, H529/F117 (amp-SH3/CD2AP SH3-2); 9, F588/161; 10, Y531/119; 11, P585/158; 12, E538/126; 13, D537/125. *B, C,* Electrostatic potential surface representations of amp-SH3 in complex with CHIKV. *D, E*, Electrostatic potential surface representations of CD2AP SH3-2 in complex with Rin3ε2. The peptides are represented in stick model. Residues E556 and E557 extend the negatively charged surface area in amp-SH3. The figure was made with the programs UCSF Chimera (1) and MOLMOL (2).

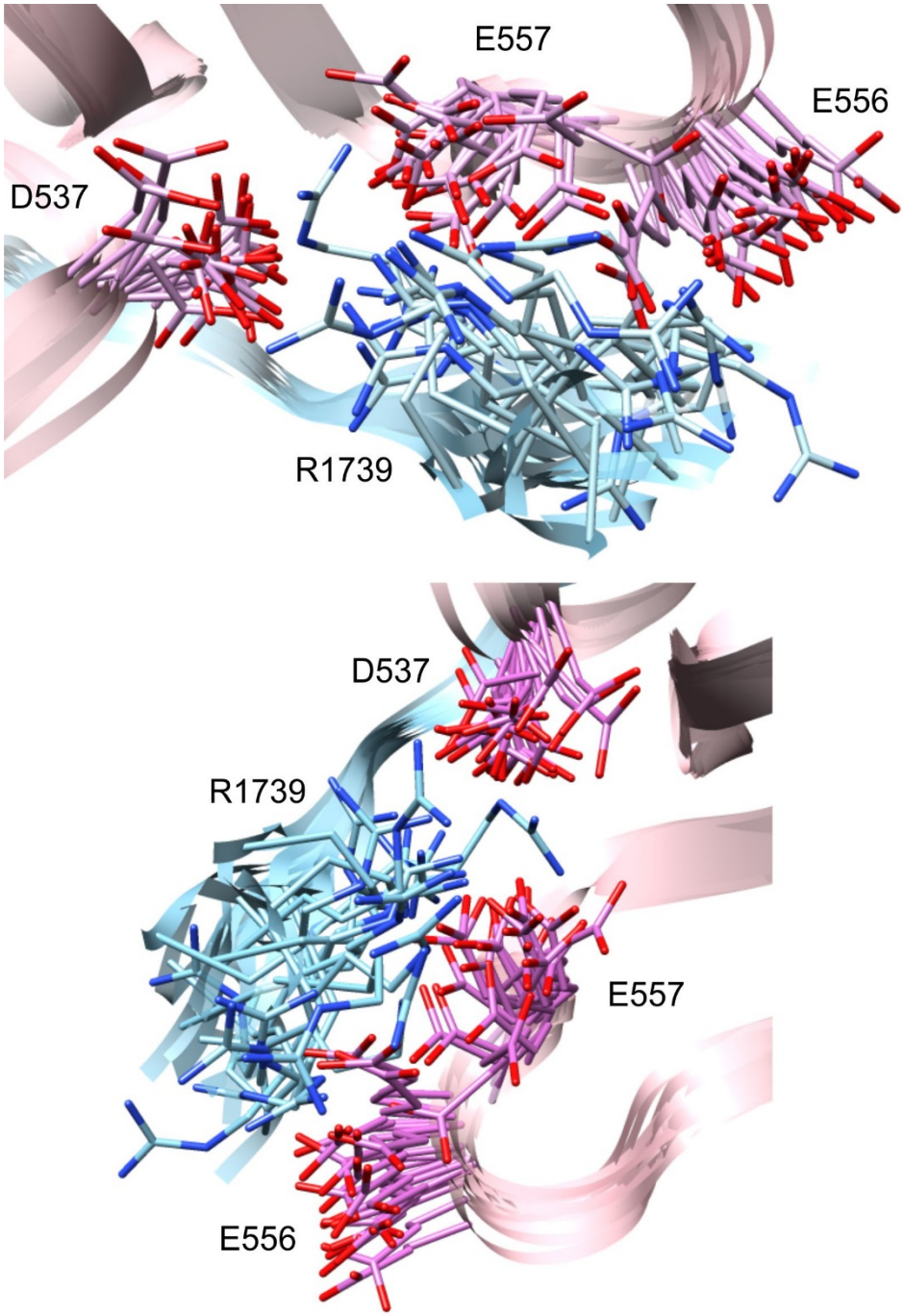

Figure S2. R1739 is a key component in the amp-SH3–CHIKV complex electrostatic interaction as indicated by the 11-fold lower affinity of the R1739A mutant. The figure shows side chain contacts between CHIKV R1739 and amp-SH3 D537 from the RT loop and E556 and E557 from the n-Src loop, in two angles of view. R1739 side chains in individual structures of the ensemble show substantial variation but are confined to the negatively charged surface created by amp-SH3 D537, E556 and E557. Hydrogens have been omitted from the figure for clarity. Figure was prepared with UCSF Chimera (2).

References

1. Pettersen, E. F., Goddard, T. D., Huang, C. C., Couch, G. S., Greenblatt, D. M., Meng, E. C., and Ferrin, T. E. (2004). UCSF Chimera--a visualization system for exploratory research and analysis. *J. Comput. Chem.* **25**, 1605-1612

2. Koradi, R., Billeter, M., and Wuthrich, K. (1996). MOLMOL: a program for display and analysis of macromolecular structures. *J. Mol. Graph.* **14**, 51-55, 29-32

Structural Basis of the High Affinity Interaction between the *Alphavirus* Nonstructural Protein-3 (nsP3) and the SH3 Domain of Amphiphysin-2

Helena Tossavainen, Olli Aitio, Maarit Hellman, Kalle Saksela and Perttu Permi

J. Biol. Chem. 2016, 291:16307-16317.
doi: 10.1074/jbc.M116.732412 originally published online June 6, 2016